JACS
JOURNAL OF THE AMERICAN CHEMICAL SOCIETY
Article
pubs.acs.org/JACS

Multifunctional π-Expanded Macrocyclic Oligothiophene 6-Mers and Related Macrocyclic Oligomers

Masahiko Iyoda,*[,†] Keita Tanaka,[†] Hideyuki Shimizu,[†] Masashi Hasegawa,[#] Tohru Nishinaga,[†] Tomohiko Nishiuchi,[†] Yoshihito Kunugi,[‡] Takayuki Ishida,[∥] Hiroyuki Otani,[⊥] Hiroyasu Sato,[¶] Koji Inukai,[§] Kazukuni Tahara,[§] and Yoshito Tobe[§]

[†]Department of Chemistry, Graduate School of Science and Engineering, Tokyo Metropolitan University, Hachioji, Tokyo 192-0397, Japan

[#]Department of Chemistry, School of Science, Kitasato University, 1-15-1 Kitasato, Minami-ku, Sagamihara, Kanagawa 252-0373, Japan

[‡]Department of Applied Chemistry, Tokai University, Hirakata, Kanagawa 259-1292, Japan

[∥]Department of Engineering Science, The University of Electro-Communications, Chofu, Tokyo182-8585, Japan

[⊥]Graduate School of Environment and Information Sciences, Yokohama National University, Hodogaya-ku, Yokohama, Kanagawa 240-8501, Japan

[¶]X-ray Research Laboratory, Rigaku Corporation, Akishima, Tokyo 196-8666, Japan

[§]Division of Frontier Materials Science, Graduate School of Engineering Science, Osaka University, Toyonaka, Osaka 560-8531, Japan

Supporting Information

ABSTRACT: Multifunctional π-expanded macrocyclic oligothiophene 6-mer **1**, as well as 9- (**2**) and 12-mers (**3**), was synthesized using a McMurry coupling reaction as the key step. The 6-mer **1** was converted to cyclo[6](2,5-thienylene-ethynylene) (**4**) by using a bromination−dehydrobromination procedure. From X-ray analysis, the crystal structures of nonplanar **1** and round-shaped **2** and **4** were elucidated. STM showed that **4** formed a self-assembled monolayer at the liquid/solid interface to produce a hexagonal porous network. Chemical oxidation of **1**, **2**, and **4** with 1 and 2 equiv of $Fe(ClO_4)_3$ produced $\mathbf{1}^{\bullet+}$ and $\mathbf{1}^{2+}$, $\mathbf{2}^{\bullet+}$ and $\mathbf{2}^{2+}$, and $\mathbf{4}^{\bullet+}$ and $\mathbf{4}^{2+}$, respectively. Although oligothiophene radical cations containing β,β-disubstituted thiophenes usually do not form π-dimers, $\mathbf{4}^{\bullet+}$ clearly formed a π-dimer owing to its planar, round shape. As for the dications of **1**, **2**, and **4**, $\mathbf{1}^{2+}$, which has 34π-electrons, exhibited a large diatropic ring current effect, whereas 34π dication $\mathbf{4}^{2+}$ only showed a medium diatropic ring current effect. In contrast to $\mathbf{1}^{2+}$ and $\mathbf{4}^{2+}$, 52π dication $\mathbf{2}^{2+}$ had biradical cationic character instead of Hückel-type cyclic conjugation. Interestingly, 6-mer **1** showed polymorphism and unusual melting point behavior due to the number of stable conformations in the solid state. Single crystals of **1** melted at 176 °C, whereas an amorphous film of **1** crystallized in the temperature range of 80−83 °C to form a lamellarly stacked microcrystalline film, which melted at 139 °C. The polymorphism of **1** was applied to either fluorescence switching or switching of field effect transistor (FET) activity and electrical conductivity.

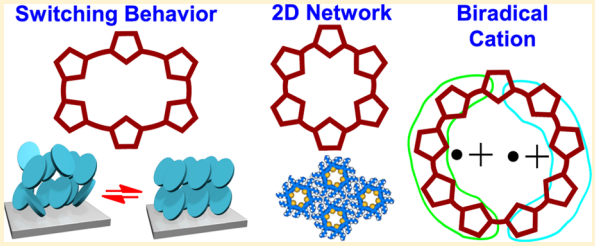

INTRODUCTION

The study of fully conjugated cyclic oligomers with precisely defined diameters has become an important tool for providing specific information on structural, electronic, and optical properties, especially in relation to "inner" and "outer" domains.[1,2] Macrocyclic structures with shape-persistent, noncollapsible, and fully π-conjugated backbones can assemble into columnar one-dimensional (1D) nanotubes,[3,4] two-dimensional (2D) porous networks, and lamellar alignments on surfaces,[5,6] and three-dimensional (3D) inclusion complexes in the solid state (Figure 1).[7,8] Furthermore, macrocycles are regarded as infinite π-conjugated systems with an inner cavity, and these π-systems have attracted considerable attention due to their unique optical and electronic behaviors with or without the perturbation of terminal substituents.[9,10] In addition, fully π-conjugated redox-active macrocycles with well-defined shapes have potential applications as switches, etc., in organic electronics.[11,12] Because these macrocycles change their charge and shape upon reduction or oxidation, the site-specific character of macrocycles can be adjusted at both their inner and outer sites. Although polymorphism of functional macrocycles has not yet been fully elucidated owing to the lack of suitable examples,[13] nanostructured polymorphs can be employed in a wide range of applications.[14]

Received: October 3, 2013
Published: January 16, 2014

   dx.doi.org/10.1021/ja4101744 | J. Am. Chem. Soc. 2014, 136, 2389−2396

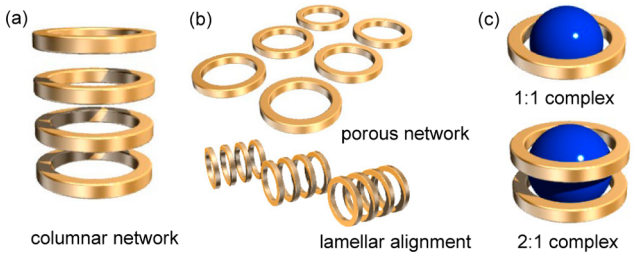

Figure 1. Possible supramolecular nanostructures of (a) 1D-, (b) 2D-, and (c) 3D-alignments of conjugated macrocycles.

Fully conjugated macrocycles were first widely investigated in the early 1960s mainly to validate theoretical calculations on annulenes with a maximum of 34π-electrons based on the Hückel rule.[15,16] Recently, we have described the synthesis of a series of giant annulenes composed of thiophene, acetylene, and ethylene building blocks.[17] Although these macrocycles can be regarded as 60π−216π annulenes without Hückel-type cyclic conjugation, the longest absorption maxima (λ_{max}) in the UV−vis spectra of 60π−216π-electron systems redshift with an increase in the ring size, indicating full conjugation of the ring. This macrocyclic conjugation gives rise to optical and electronic properties in solution.[17] Moreover, macrocycles form various nanostructures depending on their conformation and flexibility, and thus their mesophases exhibit unique functional behaviors in the solid state.[18]

Although both fully conjugated nanosized shape-persistent and flexible macrocycles are fundamentally important due to their novel structures, properties, and functions, large macrocycles are ideal molecules for the observation of single molecules, single-molecule manipulation, and single-molecule electronics.[19] We have been interested in nanostructured 1D, 2D, and 3D assemblies of conjugated macrocycles not only because the nanostructures of huge molecules can be easily detected but also because giant macrocycles stabilize mesophases to produce various nanostructured polymorphs. To investigate the relationship between the morphology and the solid-state properties of macrocycles and between the cyclic conjugation and ring size, we synthesized medium-sized macrocycles with weak Hückel-type or without Hückel-type cyclic conjugation. Herein we report on the interesting polymorphism, fluorescence switching, field effect transistor (FET) properties, and electrical conductivity of medium-sized macrocycles.

RESULTS

Synthesis. In general, repeated and thus monotonous synthetic procedures are essential for forming cyclic structures. Recently, however, many practical methods for the synthesis of macrocycles have been developed.[20] In this regard, molecular design and synthesis are key issues for constructing complex organic materials. Although some cyclic oligothiophenes have been synthesized by using the McMurry reaction,[21] we have recently found that giant macrocycles with a molecular size of >80 Å can be constructed by using a similar McMurry reaction.[17] Our preliminary experiments have shown that intramolecular pinacol coupling of **5** with a low-valent vanadium complex produces the corresponding cyclic 6-mer diol **6**. However, a Corey−Winter reaction of the diol does not yield **7** (Scheme 1).[22,23] Therefore, we prepared the oligothiophene 6-mer using a McMurry reaction of dialdehyde **8**.

Scheme 1. Pinacol Coupling of 5 with Low-Valent Vanadium

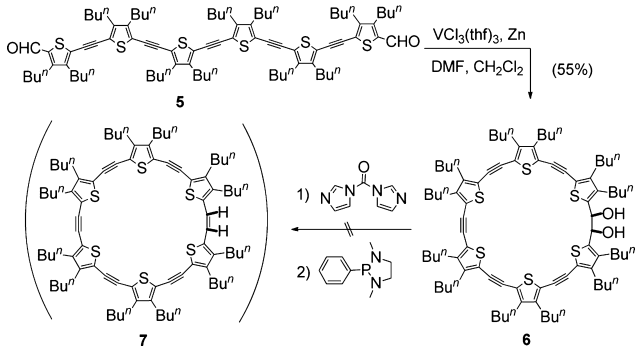

The syntheses of oligothiophene 6-mer **1** and the related higher oligomers **2** and **3** were carried out by using a modified McMurry reaction, as shown in Scheme 2. Reaction of

Scheme 2. Synthesis of π-Expanded Cyclic Oligothiophenes 1−3 and 4 Starting from Trithiophene-dialdehyde 8

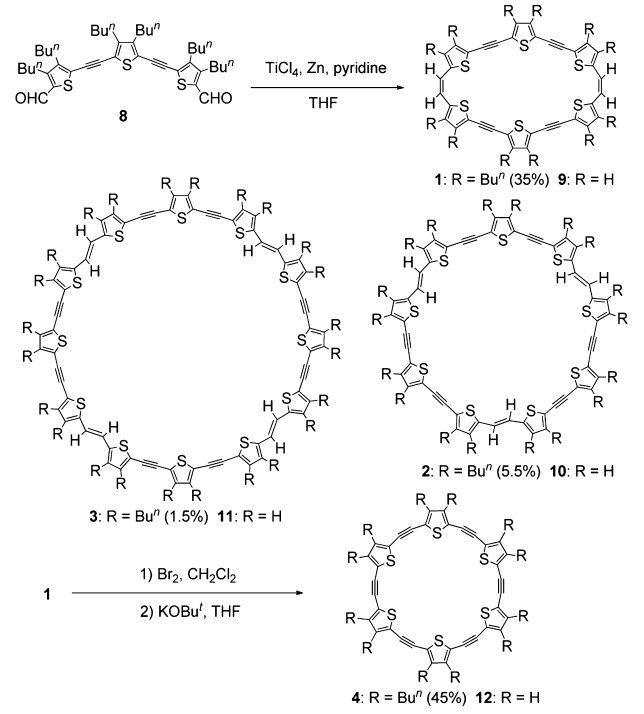

trithiophene-dialdehyde **8** with a low-valent titanium reagent generated from $TiCl_4$ and activated zinc in the presence of pyridine in THF proceeded smoothly to mainly produce cyclic dimer **1** (35%) together with cyclic trimer **2** (5.5%) and cyclic tetramer **3** (1.5%).[24] Although the formation of a small amount of cyclic pentamer **13** was observed by using laser desorption ionization time-of-flight mass spectrometry (LDI-TOF-MS), no linear di-, tri-, tetra-, or pentamers were isolated from the reaction mixture; however, higher polymers were isolated. Using this reaction, **1** was synthesized in 26% overall yield starting from easily prepared 3,4-dibutylthiophene on a gram scale. Cyclic dimer **1** was converted to cyclo[6](3,4-dibutyl-2,5-thienylene-ethynylene) **4** by using a bromination−dehydro-

dx.doi.org/10.1021/ja4101744 | J. Am. Chem. Soc. 2014, 136, 2389−2396

bromination procedure (45%). All compounds are stable red crystalline or amorphous powders and can be stored in air at room temperature for more than 1 year.

Molecular and Surface Structures. Single crystals of **1** were obtained by recrystallization from CH_2Cl_2/ethyl acetate, and its structure was determined by using X-ray analysis (Figure 2). DFT calculations on unsubstituted 6-mer **9**

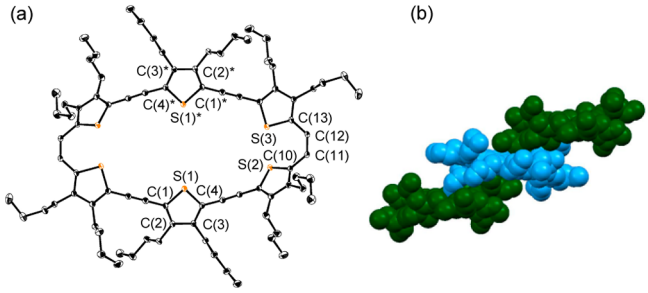

Figure 2. (a) ORTEP diagram of **1**. Torsion angle: S(2)−C(10)−C(11)−C(12) 59.49(19)°, C(11)−C(12)−C(13)−S(3) 6.5(3)°. (b) Butyl groups of **1** located above and below the macrocycle ring (light blue) in the neighboring ring (green). Thermal ellipsoids are at 50% probability. H atoms are omitted for clarity.

predicted a planar structure (Figure S14a, Supporting Information).[25] However, **1** lies on a crystallographic center of symmetry (Figure 2a), and the macroring adopts a nonplanar twisted conformation, although the two central thiophene rings (S(1)−C(1)−C(2)-C(3)−C(4) and S(1)*−C(1)*−C(2)*−C(3)*−C(4)*) are almost coplanar. The S(1)···S(1)* and S(2)···S(3) distances are 5.8272(16) Å and 3.2456(12) Å, respectively, and the latter is much shorter than the sum of S···S van der Waals radii (3.70 Å).[26] In the molecular packing of **1**, one set of butyl groups lie above and below the ring, filling the pore of the neighboring ring,[27] and the other set of butyl groups are arranged laterally without intermolecular interactions (Figure 2b). Therefore, there are no significant intermolecular $\pi-\pi$ interactions between the thiophenes of **1**. In contrast to the crystal structure of **1**, variable temperature (VT) ^{1}H NMR spectroscopy in $CDCl_3$ indicated that the structure was D_{2h}-symmetric, and there were no spectral changes at low temperature (Figure S18, Supporting Information).[28]

The molecular structure of **2** was also elucidated by using X-ray crystallographic analysis and DFT calculations (Figure S14c, Supporting Information). The peripheral butyl groups were disordered due to molecular motion even at very low temperature (Figure 3a). **2** was found to have a large π-framework with an approximately planar round shape and S···S distances in the range of 16−17 Å. In the molecular packing (Figure 3b,c), the four butyl groups sticking out of the macroring are located above or below the ring inside the neighboring ring, filling the cavity of **2**. The nearly circular structure was in reasonable agreement with the optimized structure of **10** obtained from DFT calculations (for **10**, Figure S14c, Supporting Information).

In contrast to **1** and **2**, **4** crystallized with a hexane molecule located in the center of the cavity (Figure 3d). The ring has a crystallographic inversion center at the center of the macrocycle. As shown in Figure 3d,e, the π-framework of **4** is fairly planar and circular in shape. The averaged S(1)···S(1*), S(2)···S(2*), and S(3)···S(3*) distances were found to be 9.85 Å, which is considerably close to the corresponding calculated

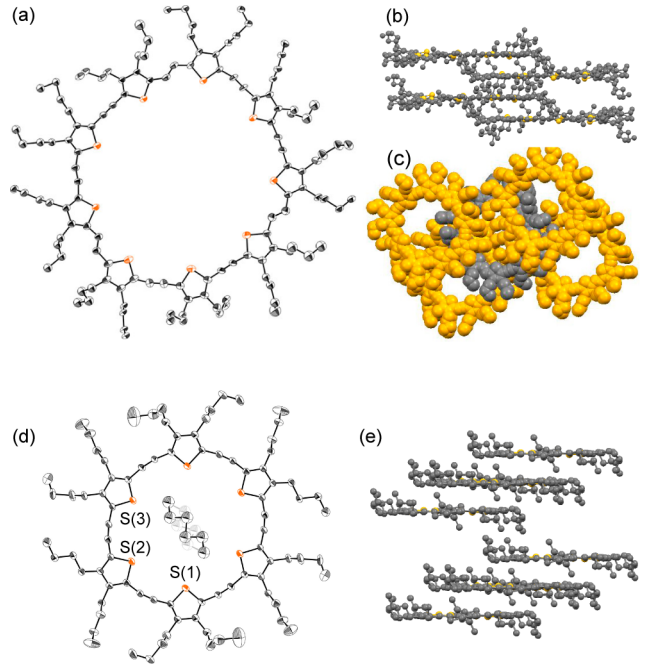

Figure 3. (a) ORTEP diagram and (b) crystal packing of **2**. (c) The four butyl groups sticking out of the neighboring four macrorings (yellow) locate in the central macroring (gray). (d) ORTEP diagram and (e) packing structure of **4**. A disordered hexane molecule is located in the center of the macroring. Thermal ellipsoids are at 10% probability for **2** and 30% probability for **4**. H atoms are omitted for clarity.

value of 9.88 Å in **12** with a C_{6h} structure (Figure S14e, Supporting Information).

Scanning tunneling microscopy (STM) revealed that planar **4** self-assembled into a monolayer at the liquid/solid interface. An STM image of the monolayer of **4** at the 1-phenyloctane/graphite interface is shown in Figure 4a. In the STM image,

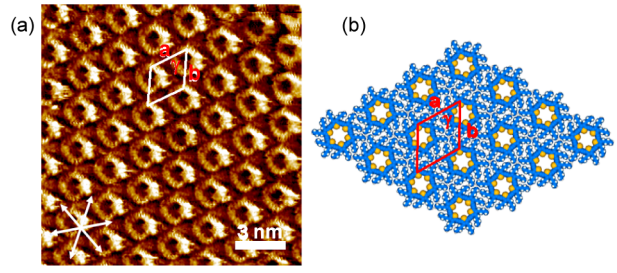

Figure 4. (a) STM image of monolayer of macrocycle **4** at a 1-phenyloctane/graphite interface (I_{set} = 0.25 nA, V_{set} = −0.56 V). (b) Tentative network model in which $a = b$ = 2.44 nm and γ = 60°.

aromatic moieties showed high tunneling efficiency, allowing straightforward interpretation of the bright/dark contrast patterns in the image.[29] In other words, the bright hexagonal features corresponded to π-electron conjugated cores, agreeing with the molecular size. The short butyl groups could not be fully resolved. Each molecule is packed hexagonally. The experimentally obtained unit cell parameters were $a = b = 2.3 \pm 0.2$ nm and $\gamma = 59 \pm 2°$. A model reflecting the molecular ordering according to the hexagonal packing is shown in Figure 4b. All molecules have the same orientation, and the short alkyl chains most likely occupy the gap between adjacent π-cores.

dx.doi.org/10.1021/ja4101744 | J. Am. Chem. Soc. 2014, 136, 2389−2396

The structure of the monolayers formed from a 1-octanoic acid solution of the macrocycle were also hexagonally packed, which is identical to that observed at the 1-phenyloctane/graphite interface. Although the butyl chains are not resolved, they most likely pack each other to fill the space between the macrocycle (Figure 4b), thus stabilizing the face-on geometry. ^{1}H NMR spectra of 0.5 mM, 1 mM, and 5 mM solutions of **4** in CD_2Cl_2 at −5 °C showed no spectral changes, indicating that there were no $\pi-\pi$ stacking interactions in the CD_2Cl_2 solutions (Figure S19, Supporting Information). Consistently, the formation of an edge-on structure[30] or a second adsorbate layer,[31] which are observed for substrates that tend to stack each other, was not observed in the case of **4**.

Electrochemistry. In general, oligothiophenes are relatively easy to oxidize because of their high HOMO levels. In the cyclic voltammograms (CVs) of **1**−**4** (Figure S15, Supporting Information), reversible waves corresponding to first and second oxidation processes were observed at low potentials, which is consistent with other oligothiophenes (Table 1).

Table 1. Oxidation Potentials[a] of 1−4 and HOMO Levels of Corresponding Unsubstituted Macrocycles 9−12

compd	$E^{ox1}_{1/2}$ (V)	$E^{ox2}_{1/2}$ (V)	HOMO (eV)[b]	HOMO (eV)[c]
1	0.33, 2e	−[d]	−5.17	−4.70 for D_{2h}-**9**
2	0.27, 1e	0.56, 1e	−5.11	−4.82 for C_{3h}-**10**
3	0.27, 1e	0.56, 1e	−5.11	−4.69 for C_{4h}-**11**
4	0.34, 1e	0.59, 1e	−5.18	−4.91 for C_{6h}-**12**

[a]Determined from CVs under the following conditions: 0.1 M *n*-Bu_4NPF_6 in 1,2-dichloroethane, Ag/AgCl reference electrode, Pt disc as working electrode, Pt wire as counter-electrode, 0.02 V s^{-1}, 25 °C; V vs F_c/F_c^+. [b]HOMO energy value was deduced from the measured $E^{ox1}_{1/2}$. [c]HOMO level was estimated at the B3LYP/6-31G(d,p) level. [d]No second oxidation peak was observed.

Although **1** exhibited one two-electron oxidation due to weak on-site-Coulombic repulsion between the positive charges and aromatic stability of $\mathbf{1}^{2+}$, **2**, **3**, and **4** showed two one-electron oxidations.[32] The calculated HOMO levels of **9**−**12** at the B3LYP/6-31G(d,p) level were slightly higher than the estimated HOMO levels from the oxidation potentials of **1**−**4** and the energy level of F_c/F_c^+ couple to vacuum (−4.84 eV).[33]

Chemical Oxidations of 1, 2, and 4. Considering that **1**, **2**, and **4** have low oxidation potentials and peripheral 36 (for **1** and **4**) and 54 (for **2**) π-elecrtrons,[34] they can be oxidized to produce the corresponding stable cationic species. Before this study, the effect of the ring size and shape of cyclic radical cations on π-dimer formation was unknown. Furthermore, cyclic dications can show Hückel-type diamagnetic ring currents or open-shell biradical cationic character, which leads to unique optical and magnetic properties.[35] Although **2** and **3** showed similar UV−vis spectra to the reported oligothiophene 10- and 12-mers,[17] the UV−vis spectra of **1** and **2** exhibited weak S0→S1 and strong S0→S2 absorptions (Figure 5, and Figure S16a, Supporting Information). When an orange solution of **1** in $CH_2Cl_2-CH_3CN$ (9:1) was oxidized with 1 and 2 equiv of $Fe(ClO_4)_3$,[36] dark brown and deep-blue solutions of the radical cation $\mathbf{1}^{\bullet+}$ and dication $\mathbf{1}^{2+}$, respectively, were obtained. In the UV−vis−NIR spectrum of $\mathbf{1}^{2+}$, sharp, intense absorptions were observed at λ_{max} = 593 and 1185 nm (Figure 5a), which is typical for dications with a closed shell structure with no ESR signal,[37,38] whereas in the UV−vis-NIR

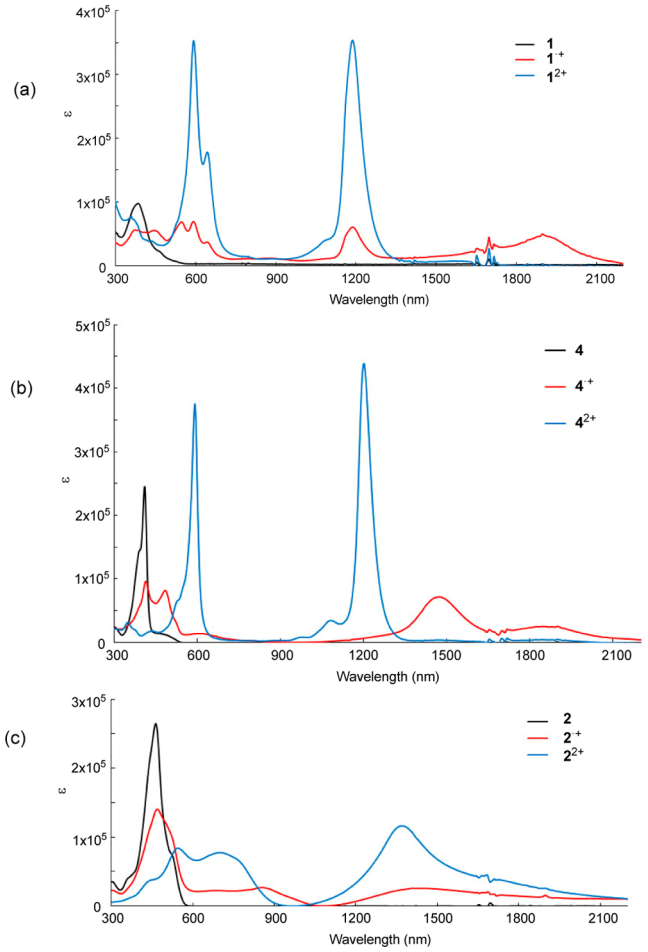

Figure 5. UV−vis-NIR spectra of (a) **1**, $\mathbf{1}^{\bullet+}$, and $\mathbf{1}^{2+}$, (b) **4**, $\mathbf{4}^{\bullet+}$, and $\mathbf{4}^{2+}$, and (c) **2**, $\mathbf{2}^{\bullet+}$, and $\mathbf{2}^{2+}$ in $CH_2Cl_2-CH_3CN$ (9:1) at 5 °C. Concentration: 6.00 × 10^{-5} mol L^{-1}; oxidant: $Fe(ClO_4)_3$; 1 mm quartz cell.

spectrum of $\mathbf{1}^{\bullet+}$, a broad absorption centered at 1910 nm and weak absorptions for $\mathbf{1}^{2+}$ at λ_{max} = 593 and 1185 nm (Figure 5a, and Figure S20, Supporting Information) were observed because $\mathbf{1}^{\bullet+}$ was easily oxidized to $\mathbf{1}^{2+}$, which agrees with the CV data. Similarly, **4** was oxidized with 1 and 2 equiv of $Fe(ClO_4)_3$ in $CH_2Cl_2-CH_3CN$ (9:1), which first afforded a brown solution of the radical cation $\mathbf{4}^{\bullet+}$ with λ_{max} = 1480 and 1850 nm, followed by a bluish violet solution of the dication $\mathbf{4}^{2+}$ with λ_{max} at 593 and 1200 nm (Figure 5b, and Figure S22a, Supporting Information).[38] Temperature-dependent UV−vis−NIR measurements on $\mathbf{4}^{\bullet+}$ showed an increase in the band at 1480 nm (π-dimer absorption) and a decrease in the band at 1850 nm (monomer absorption) with a decrease in the temperature (Figure S22b, Supporting Information). In addition, the intensity of the ESR signal for $\mathbf{4}^{\bullet+}$ at g = 2.0024 at 7 °C decreased with a decrease in the temperature, and the peak disappeared at −93 °C (Figure S23, Supporting Information). The spectral changes were completely reversible, clearly indicating that a π-dimer of $\mathbf{4}^{\bullet+}$ ($(\mathbf{4}^{\bullet+})_2$) formed. To the best of our knowledge, no oligothiophene radical cations containing β,β-disubstituted thiophene rings have been reported to form a π-dimer even at low temperature due to steric repulsion.[39] Thus, $(\mathbf{4}^{\bullet+})_2$ is the first example of a π-dimer of β,β-disubstituted thiophene oligomers. In the UV−vis−NIR spectrum of dication $\mathbf{4}^{2+}$, sharp, intense absorptions at λ_{max} =

dx.doi.org/10.1021/ja4101744 | J. Am. Chem. Soc. 2014, 136, 2389−2396

592 and 1201 nm were observed (Figure 5b), and no ESR signals were observed, indicating the formation of a closed shell dication.

In contrast to the UV−vis−NIR spectra of $\mathbf{1}^{2+}$ and $\mathbf{4}^{2+}$, the spectrum of $\mathbf{2}^{2+}$ indicated biradical cationic character (Figure 5c, and Figure S25, Supporting Information). Oxidation of **2** with 1 equiv of $Fe(ClO_4)_3$ in CH_2Cl_2−CH_3CN (9:1) produced a brown solution of $\mathbf{2}^{\bullet+}$, which showed a spectrum similar to those of $\mathbf{1}^{\bullet+}$ and $\mathbf{4}^{\bullet+}$. However, very broad absorptions ($\lambda^{\text{longest}}_{\text{max}}$ = 1361 nm) were observed for doubly oxidized violet $\mathbf{2}^{2+}$, like that for the radical cation $\mathbf{2}^{\bullet+}$. Because the ESR spectrum of $\mathbf{2}^{\bullet+}$ (g = 2.0024 at 7 °C) is similar to that of $\mathbf{2}^{2+}$ (g = 2.0026 at 7 °C) (Figures S26 and S27, Supporting Information), the biradical state of $\mathbf{2}^{2+}$ is nearly equivalent to that of two independent monoradicals having a small exchange interaction. As for $\mathbf{2}^{\bullet+}$, the intensity of the ESR signal first decreased with a decrease in the temperature down to −103 °C (Figure S26, Supporting Information) and then increased again at −113 °C,[40] and the UV−vis−NIR spectra of $\mathbf{2}^{\bullet+}$ at 20 and −20 °C were nearly the same (Figure S28a, Supporting Information). Therefore, $\mathbf{2}^{\bullet+}$ did not form a π-dimer presumably due to weaker SOMO−SOMO interactions in the 53π radical cation $\mathbf{2}^{\bullet+}$ than those in 33π radical cation $\mathbf{4}^{\bullet+}$. In contrast to $\mathbf{1}^{2+}$ and $\mathbf{4}^{2+}$, $\mathbf{2}^{2+}$ exhibited an ESR signal owing to a thermally excited triplet state, and the signal remained even at −113 °C. The ESR signals of $\mathbf{2}^{\bullet+}$ and $\mathbf{2}^{2+}$ were similar; however, the peak-to-peak widths for $\mathbf{2}^{\bullet+}$ and $\mathbf{2}^{2+}$ at 7 °C were 3.32 and 4.59 G, respevtively. Furthermore, the UV−vis−NIR spectra of $\mathbf{2}^{2+}$ at 20 and −20 °C were similar (Figure S28b, Supporting Information), although the ε values were different. The spectral results confirmed the presence of a biradical cation. The amplitude of the biradical character of $\mathbf{10}^{2+}$ was calculated to be 99% by NOON (natural orbital occupation number) analysis at the UB3LYP/6-31G(d,p) level.[41]

In ^{1}H NMR spectra of $\mathbf{1}^{2+}$, which was prepared by oxidation with 2 equiv of $Fe(ClO_4)_3$ at 0 °C, in CD_2Cl_2−CD_3CN (9:1) at −10 °C, the peak for the olefin proton of the 34π-electron diamagnetic system was shifted downfield (δ 13.69) (NICS(1) (nucleus-independent chemical shift (1) = −16.1) from that of atropic **1** (δ 6.61) (NICS(1) = 0.91) (Figure S21, Supporting Information).[42] On the other hand, the oxidation of **4** with 2 equiv of $Fe(ClO_4)_3$ in CD_2Cl_2−CD_3CN (9:1) afforded $\mathbf{4}^{2+}$, which has weaker diamagnetic ring currents. In the ^{1}H NMR spectrum of $\mathbf{4}^{2+}$ at −10 °C, the peak for the methylene protons attached to thiophenes (δ 4.07) (NICS(1) = −15.6) were moderately shifted downfield compared to the corresponding protons of **4** (δ 2.47) (NICS(1) = 0.68) (Figure S24, Supporting Information). The chemical shifts of the corresponding methylene protons of **1** and $\mathbf{1}^{2+}$ were δ 2.49−2.63 and 5.74−6.46, respectively. Restraint on the Hückel-type diamagnetic ring currents of the macrocycles with an acetylene linkage has been reported on dehydroannulenes (bond localization effect).[16a] As expected from the ESR spectrum, in ^{1}H NMR spectra of $\mathbf{2}^{2+}$, broad signals due to the radical species were observed.

Polymorphism. The most interesting property of π-expanded oligothiophenes reported here is the polymorphism of 6-mer **1**. As shown in Figure 6a, single crystals of **1** corresponding to the X-ray structure (Figure 2) melted at 176 °C in the first heating process (blue line, ΔH = 81.8 kJ mol^{-1}), determined by using differential scanning calorimetry (DSC) analysis (Figure S33, Supporting Information). When cooled to room temperature, **1** formed an amorphous solid. However, in

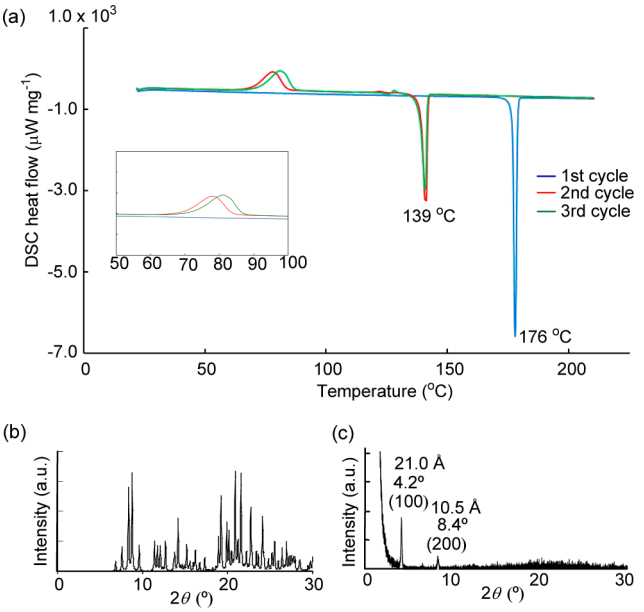

Figure 6. (a) DSC analysis of **1** (2 °C/min). The inset shows the region 50 < T < 100 °C. (b) XRD pattern for a powder sample of **1** using the single crystal data. (c) XRD pattern for **LC-1**, indicating a laterally ordered structure (d = 21.0 Å) that rises 54° diagonally from the aluminum plate used for the XRD analysis. In contrast, **AF-1** showed no reflections (Figure S43a, Supporting Information).

the second heating process, **1** showed an exothermic process (red line in the inset, ΔH = −39.8 kJ mol^{-1}) at 80 °C to form crystals that melted at 139 °C (ΔH = 53.9 kJ mol^{-1}) (Figure S34, Supporting Information),[43] and in the third heating process, an exothermic process with a melt memory effect (green line in the inset, ΔH = −37.9 kJ mol^{-1}) occurred at 83 °C to form crystals that melted again at 139 °C (ΔH = 50.8 kJ mol^{-1}) (inset). On the basis of the analysis of the exothermic process by changing the heating and cooling rates, we concluded that the difference of the exothermic temperature (inset in Figure 6a) was due to the thickness of the sample on the surface.[44] X-ray diffraction (XRD) patterns for the single crystals and crystals melting at 139 °C were completely different (Figure 6b,c). As shown in Figure 6c, crystals melting at 139 °C consisted of lamellarly aligned molecules of **1** (**LC-1**) on the glass and metal surfaces.[45] Thus, **1** has three solid-state structures: single crystal, lamellar film, and amorphous film (**AF-1**). This polymorphism was only observed for **1** due to the number of stable conformations in the solid state, whereas the cast films of **2**, **3**, and **4** formed amorphous solids and exhibited decomposition without showing a melting point.[46] Because crystal structures should be ordered in the crystal lattice, **1** adopts a twisted structure in the single crystal. However, the formation of an edge-on structure is favorable on the surface through π−π stacking interaction, and consequently, we assumed that **1** adopts a lamellarly aligned structure on the glass and metal surfaces.[47]

Polymorphs of **1** have different optical and electronic properties.[48] In Table 2, absorption and emission spectra, XRD reflections, FET behavior, and electrical conductivity of **AF-1** and **LC-1** on the surfaces of glass and metal plates are summarized. The absorption and emission spectra of **LC-1** were red-shifted compared to those of **AF-1** due to an increase in the π−π interactions (Figure 7a, Figures S37 and S38, Supporting Information). The colors of **AF-1** and **LC-1** are

dx.doi.org/10.1021/ja4101744 | J. Am. Chem. Soc. 2014, 136, 2389−2396

Table 2. Optical and Electronic Properties of Amorphous Films (AF-1) and Lamellarly Aligned Microcrystals (LC-1) of 1 on the Surface of Glass and Metal Plates

	AF-1	LC-1
absorption (nm)[a]	384	418, 425*, 510*
emission (nm, Φ_F)[b]	607 (Φ_F = 1.3%)	674 (Φ_F < 0.5%)
XRD (2θ, deg)	–[c]	4.2, 8.4
FET (μ, cm^2 V^{-1} s^{-1})	–[d]	2.8×10^{-3}
conductivity (σ, S cm^{-1})[e]	2.6×10^{-10}	4.0×10^{-7}
after I_2-doping (σ)[f]	2.5×10^{-5}	1.1×10^{-2}

[a]Asterisk indicates a shoulder. [b]Absolute fluorescence quantum yield. [c]No reflection was observed. [d]No FET property was observed. [e]Electrical conductivity measured by a two-probe method at room temperature. [f]Doped with saturated I_2 vapor for 1–2 min and measured by using a two-probe method at room temperature.

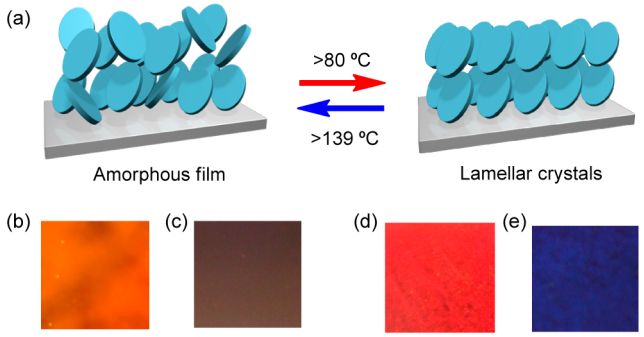

Figure 7. (a) Schematic representation of the polymorphism of amorphous film **AF-1** and lamellarly stacked crystalline film **LC-1** on substrate surfaces. (b) The color of **AF-1**, (c) the color of **AF-1** under UV-light irradiation (λ = 254 nm), (d) the color of **LC-1**, and (e) the color of **LC-1** under UV-light irradiation (λ = 254 nm).

orange and reddish orange, respectively (Figure 7b,d), consistent with the absorption spectra. The colors of **AF-1** and **LC-1** under UV-light (λ = 254 nm) were also different (Figure 7c,e), and **AF-1** fluoresced, whereas **LC-1** only exhibited weak emission. The π–π stacked structure of **LC-1** showed FET properties ($\mu = 2.8 \times 10^{-3}$ cm^2 V^{-1} s^{-1}, $I_{on}/I_{off} = 10^4$, and $V_{th} = -4.7$ V) and an increased conductivity ($\sigma_{rt} = 4.0 \times 10^{-7}$ Scm^{-1}) compared with that of **AF-1** ($\sigma_{rt} = 2.6 \times 10^{-10}$ S cm^{-1}). Furthermore, after doping with iodine, the conductivities of **AF-1** and **LC-1** (2.5×10^{-5} and 1.1×10^{-2} Scm^{-1}, respectively) were higher than those of the corresponding neutral films, and the conductivity of doped **LC-1** was 440-times higher than that of doped **AF-1**.

The polymorphism and unusual melting point behavior of **1** can be used in the design of molecular switches. **AF-1** on a quartz plate had a fluorescent, amorphous morphology (Figure 7c). When the film was heated at 100 °C for 10 min, crystallization occurred to produce weakly fluorescent **LC-1** (Figure 7e). **LC-1** could be converted to **AF-1** by heating above the melting point (139 °C). **AF-1** fluoresced with λ_{max} = 607 nm and showed very low conductivity and no FET properties due to its lack of π–π stacked thiophene units. On the other hand, **LC-1** weakly fluoresced with λ_{max} = 674 nm and showed an increased conductivity and FET properties due to its J-aggregated structure.[49] Strikingly, the conversion between **AF-1** and **LC-1** could be repeated several times by heating either at 100 °C for 10 min or above melting point, as shown in Figure 8 and Figure S39, Supporting Information. After five cycles, there was no change in the intensity of the emissions at 550 and 750

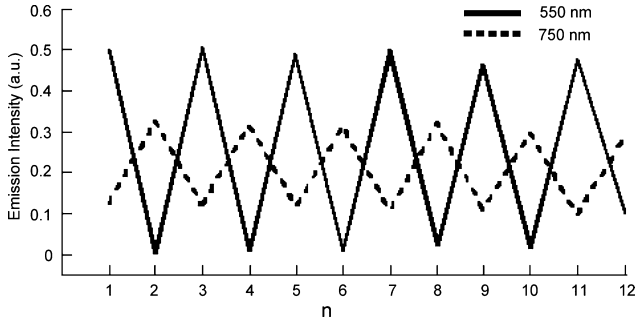

Figure 8. Normalized relative emission intensities of **AF-1** and **LC-1** measured at 550 nm (solid line) and 750 nm (dotted line), respectively, at 23 °C. After heating above the melting point (139 °C), the emissions at 550 and 750 nm were measured at n = 1, 3, 5, 7, 9, and 11, and after heating at 100 °C for 10 min, the emissions at 550 and 750 nm were measured for n = 2, 4, 6, 8, 10, and 12.

nm. Moreover, FET properties and conductivity of the **AF-1** and **LC-1** states could be reproduced several times without attenuation of the ON/OFF ratio of the FET properties and conductivity. Furthermore, the iodine adsorption/desorption behavior of **AF-1** and **LC-1** led to a reversible change in the electrical conductivity, meaning that the conductivity could be switched between those of **AF-1** and **LC-1** repeatedly.

CONCLUSION

In summary, the medium-sized macrocyclic oligothiophene 6-mer **1** was synthesized together with small amounts of 9-mer **2** and 12-mer **3** by cyclization of thiophene-dialdehyde **8** with a low-valent titanium reagent, and the bromination–dehydrobromination procedure of **1** produced cyclo[6](3,4-dibutyl-2,5-thienylene-ethynylene) **4**. X-ray analysis of **1**, **2**, and **4** showed that **1** adopted a nonplanar twisted elliptical structure, and **2** and **4** had planar round shapes. In the crystal of **4**, a disordered hexane occupied the center of the cavity, whereas the cavities of **1** and **2** were filled by the butyl groups of the neighboring macrorings. STM revealed that hexagonal **4** formed a self-assembled monolayer at the liquid/solid interface to produce a hexagonal porous network. The HOMO levels of **1**, **2**, and **4** are high in energy, and thus, they have low oxidation potentials. In other words, **1**, **2**, and **4** could be chemically oxidized with 1 and 2 equiv $Fe(ClO_4)_3$, affording the corresponding radical cations $\mathbf{1}^{\bullet+}$, $\mathbf{2}^{\bullet+}$, and $\mathbf{4}^{\bullet+}$ and dicatons $\mathbf{1}^{2+}$, $\mathbf{2}^{2+}$, and $\mathbf{4}^{2+}$. Although $\mathbf{1}^{\bullet+}$ rapidly oxidized to $\mathbf{1}^{2+}$, $\mathbf{2}^{\bullet+}$ and $\mathbf{4}^{\bullet+}$ could be characterized spectroscopically. Temperature-dependent ESR and UV–vis-NIR spectroscopies revealed that $\mathbf{4}^{\bullet+}$ formed π-dimer at low temperatures, whereas $\mathbf{2}^{\bullet+}$ did not. $(\mathbf{4}^{\bullet+})_2$ is the first example of a π-dimer generated from β,β-disubstituted thiophene oligomers. **1** and **4** maintained Hückel-type cyclic conjugation and formed closed-shell 34π dications $\mathbf{1}^{2+}$ and $\mathbf{4}^{2+}$, both of which showed fairly large diamagnetic ring currents. In contrast, 9-mer **2** produced non-Hückel-type dication $\mathbf{2}^{2+}$, which consists of two radical cations. NOON analysis at the UB3LYP/6-31G(d,p) level confirmed that the radical cation pair structure was more stable than that of the closed-shell 52π dication. Unlike **2** and **4**, **1** exhibited polymorphism in the solid state. Although **1** formed single crystals from CH_2Cl_2–ethyl acetate, the crystals melted at 176 °C to produce an amorphous film (**AF-1**) at room temperature, affording a lamellarly aligned microcrystalline structure (**LC-1**) at 80 °C, which melted at 139 °C. These three solid phases of **1** showed different functional properties, and the thermally reversible interconver-

dx.doi.org/10.1021/ja4101744 | J. Am. Chem. Soc. 2014, 136, 2389–2396

sion between **AF-1** and **LC-1** was studied from the viewpoint of on/off fluorescence, FET behavior, and conductivity experiments. Furthermore, I_2 doping caused the conductivity of **AF-1** and **LC-1** to increase, and the conductivity of the I_2-doped **LC-1** (σ_{rt} = 1.1 × 10^{-2} S cm^{-1}) was 440-times higher than that of the I_2-doped **AF-1**.

■ ASSOCIATED CONTENT

Supporting Information

Experimental procedures and the characterization data of **1**−**4** and **8**; Figures S1−S43; Scheme S1; Tables S1−S11; Cartesian coordinates and total energies of the optimized structures of all calculated molecules (B3LYP/6-31G(d,p)); crystallographic information files (CIF) for **1**, **2**, and **4**. This material is available free of charge via the Internet at http://pubs.acs.org.

■ AUTHOR INFORMATION

Corresponding Author

iyoda@tmu.ac.jp

Notes

The authors declare no competing financial interest.

■ ACKNOWLEDGMENTS

This work was partly supported by a Grant-in-Aid for Scientific Research on Innovative Areas "Reaction Integration" and by CREST of JST (Japan Science and Technology Corporation). We thank Mr. Shun Sugibayashi, Dr. Eigo Isomura, and Dr. Jun Yamakawa (Tokyo Metropolitan University) for their experimental assistance and Ms. Chinatsu Kobayashi (Tokai University) for the measurements of the FET behavior of **1**. We also thank Prof. Hirohisa Yoshida and Mr. Jang Junhyeok (Tokyo Metropolitan University) for their assistance with DSC and XRD measurements. We are thankful to Dr. Masayoshi Takase (Tokyo Metropolitan University), Prof. Gaku Yamamoto (Kitasato University), and Prof. Takashi Kubo (Osaka University) for helpful discussions.

■ REFERENCES

(1) For reviews: (a) Iyoda, M.; Yamakawa, J.; Rahman, M. J. *Angew. Chem., Int. Ed.* **2011**, *50*, 10522−10553. (b) Höger, S. *Chem.—Eur. J.* **2004**, *10*, 1320−1329.

(2) (a) Krömer, J.; Rios-Carreras, I.; Fuhrmann, G.; Musch, C.; Wunderlin, M.; Debaerdemaeker, T.; Mena-Osteritz, E.; Bäuerle, P. *Angew. Chem., Int. Ed.* **2000**, *39*, 3481−3486. (b) Kawase, T.; Tanaka, K.; Seirai, Y.; Shiono, N.; Oda, M. *Angew. Chem., Int. Ed.* **2003**, *42*, 5597−5600. (c) Jung, S.-H.; Pisula, W.; Rouhanipour, A.; Räder, H. J.; Jacob, J.; Müllen, K. *Angew. Chem., Int. Ed.* **2006**, *45*, 4685−4690. (d) Hoffmann, M.; Wilson, C. J.; Odell, B.; Anderson, H. L. *Angew. Chem., Int. Ed.* **2007**, *46*, 3112−3125. (e) Mössinger, D.; Chaudhuri, D.; Kudernac, T.; Lei, S.; De Feyter, S.; Lupton, J. M.; Höger, S. *J. Am. Chem. Soc.* **2010**, *132*, 1410−1423.

(3) For reviews: (a) Hoeben, F. J. M.; Jonkheijm, P.; Meijer, E. W.; Schenning, P. H. J. *Chem. Rev.* **2005**, *105*, 1491−1546. (b) Zang, L.; Che, Y.; Moore, J. *Acc. Chem. Res.* **2008**, *41*, 1596−1608. (c) De Greef, T. F. A.; Smulders, M. M. J.; Wolffs, M.; Schenning, A. P. H. J.; Sijbesma, R. P.; Meijer, E. W. *Chem. Rev.* **2009**, *109*, 5687−5754.

(4) (a) Yamamoto, T.; Fukushima, T.; Yamamoto, Y.; Kosaka, A.; Jin, W.; Ishii, N.; Aida, T. *J. Am. Chem. Soc.* **2006**, *128*, 14337−14340. (b) Bong, D. T.; Clark, T. D.; Granja, J. R.; Ghadiri, M. R. *Angew. Chem., Int. Ed.* **2001**, *40*, 988−1011. (c) Kogiso, M.; Ohnishi, S.; Yase, K.; Masuda, M.; Shimizu, T. *Langmuir* **1998**, *14*, 4978−4986. (d) Ghadiri, M. R.; Granja, J. R.; Milligan, R. A.; McRee, D. E.; Khazanovich, N. *Nature* **1993**, *366*, 324−327.

(5) For reviews: (a) Kudernac, T.; Lei, S.; Elemans, J. A. A. W.; De Feyter, S. *Chem. Soc. Rev.* **2009**, *38*, 402−421. (b) Höger, S. *Pure Appl. Chem.* **2010**, *82*, 821−830. (c) Mohnani, S.; Bonifazi, D. *Coord. Chem. Rev.* **2010**, *254*, 2342−2362.

(6) (a) Tahara, K.; Lei, S.; Mamdouh, W.; Yamaguchi, Y.; Ichikawa, T.; Uji-I, H.; Sonoda, M.; Hirose, K.; De Schryver, F. C.; De Feyter, S.; Tobe, Y. *J. Am. Chem. Soc.* **2008**, *130*, 6666−6667. (b) Mena-Osteritz, E.; Bäuerle, P. *Adv. Mater.* **2006**, *18*, 447−451. (c) Pan, G.-B.; Chen, X.-H.; Höger, S.; Freyland, W. *J. Am. Chem. Soc.* **2006**, *128*, 4218−4219.

(7) For reviews: (a) Kawase, T.; Kurata, H. *Chem. Rev.* **2006**, *106*, 5250−5273. (b) Kawase, T.; Oda, M. *Pure Appl. Chem.* **2006**, *77*, 831−839. (c) Tahara, K.; Tobe, Y. *Chem. Rev.* **2006**, *106*, 5274−5290.

(8) (a) Rahman, M. J.; Shimizu, H.; Araki, Y.; Ikeda, H.; Iyoda, M. *Chem. Commun.* **2013**, *49*, 9251−9253. (b) Hubble, L. J.; Raston, C. L. *Chem.—Eur. J.* **2007**, *13*, 6755−6760.

(9) (a) *Electronic Materials: The Oligomer Approach*; Müllen, K.; Wegner, G., Eds.; Wiley-VCH, Weinheim, 1998. (b) Babudri, F.; Farinola, G. M.; Naso, F. *J. Mater. Chem.* **2004**, *14*, 11−34. (c) Cuesta, L.; Sessler, J. L. *Chem. Soc. Rev.* **2009**, *38*, 2716−2729.

(10) For recent reviews of π-conjugated macrocycles: (a) Grave, C.; Schlüter, A. D. *Eur. J. Org. Chem.* **2002**, 3075−3098. (b) Yamaguchi, Y.; Yoshida, Z. *Chem.—Eur. J.* **2003**, *9*, 5430−5440. (c) Young, D. Z.; Moore, J. S. *Chem. Commun.* **2003**, 807−818. (d) Höger, S. *Chem.—Eur. J.* **2004**, *10*, 1320−1329. (e) Spitler, E. L.; Johnson, C. A., II; Haley, M. M. *Chem. Rev.* **2006**, *106*, 5344−5386. (f) Zhang, W.; Moore, J. S. *Angew. Chem., Int. Ed.* **2006**, *45*, 4416−4439. (g) Höger, S. *Acetylene Chemistry*; Diederich, F.; Stang, P. J.; Tykwinski, R. R., Eds.; Wiley-VCH: Weinheim, 2005; pp 427−452. (h) *Modern Supramolecular Chemistry: Strategies for Macrocycle Synthesis*; Diederich, F.; Stang, P. J.; Tykwinski, R. R., Eds.; Wiley-VCH: Weinheim, 2008.

(11) (a) Grimsdale, A. C.; Müllen, K. *Angew. Chem., Int. Ed.* **2005**, *44*, 5592−5629. (b) *Carbon-Rich Compounds, From Molecules to Materials*; Haley, M. M.; Tykwinski, R. R, Eds.; Wiley-VCH: Weinheim, 2006. (c) Wu, J.; Pisula, W.; Müllen, K. *Chem. Rev.* **2007**, *107*, 718−747.

(12) (a) Schmaltz, B.; Rouhanipour, A.; Räder, H. J.; Pisula, W.; Müllen, K. *Angew. Chem., Int. Ed.* **2009**, *48*, 720−724. (b) Zhang, F.; Götz, G.; Winkler, H. D. F.; Schalley, C. A.; Bäuerle, P. *Angew. Chem., Int. Ed.* **2009**, *48*, 6632−6635. (c) Bhaskar, A.; Ramakrishna, G.; Hagedorn, K.; Varnavski, O.; Mena-Osteritz, E.; Bäuerle, P.; Goodson, T., III. *J. Phys. Chem. B* **2007**, *111*, 946−954. (d) Köhler, B.; Enkelmann, V.; Oda, M.; Pieraccini, S.; Spada, G. P.; Scharf, U. *Chem.—Eur. J.* **2001**, *7*, 3000−3004.

(13) (a) Miller, Y.; Ma, B.; Nussinov, R. *Chem. Rev.* **2010**, *110*, 4820−4838. (b) Sommerdijk, N. A. J. M.; de With, G. *Chem. Rev.* **2008**, *108*, 4499−4550. (c) Desiraju, G. R. *Angew. Chem., Int. Ed.* **2007**, *46*, 8342−8356.

(14) (a) Nangia, A. *Acc. Chem. Res.* **2008**, *41*, 595−604. (b) Darling, S. B. *Prog. Polym. Sci.* **2007**, *32*, 1152−1204.

(15) (a) Iyoda, M.; Nakagawa, M. *Tetrahedron Lett.* **1973**, 4743−4746. (b) Ojima, J.; Fujita, S.; Masumoto, M.; Ejiri, E.; Kato, T.; Kuroda, S.; Nozawa, Y.; Tatemitsu, H. *J. Chem. Soc. Chem. Commun.* **1987**, 534−536.

(16) Recent reviews: (a) Mitchell, R. H. *Chem. Rev.* **2001**, *101*, 1301−1315. (b) Kennedy, R. D.; Lloyd, D.; McNab, H. *J. Chem. Soc., Perkin Trans. 1* **2002**, 1601−1621. (c) Marsella, M. J. *Acc. Chem. Res.* **2002**, *35*, 944−951. (d) Marsden, J. A.; Palmer, G. J.; Haley, M. M. *Eur. J. Org. Chem.* **2003**, 2355−2369. (e) Spitler, E. L.; Johnson, C. A., II; Haley, M. M. *Chem. Rev.* **2006**, *106*, 5344−5386. (f) Nishinaga, T. *Sci. Synth.* **2009**, *45a*, 407−427.

(17) (a) Nakao, K.; Nishimura, M.; Tamachi, T.; Kuwatani, Y.; Miyasaka, H.; Nishinaga, T.; Iyoda, M. *J. Am. Chem. Soc.* **2006**, *128*, 16740−16747. (b) Williams-Harry, M.; Bhaskar, A.; Ramakrishna, G.; Goodson, T., III; Imamura, M.; Mawatari, A.; Nakao, K.; Enozawa, H.; Nishinaga, T.; Iyoda, M. *J. Am. Chem. Soc.* **2008**, *130*, 3252−3253.

(18) (a) Iyoda, M. *C. R. Chim.* **2009**, *12*, 395−402. (b) Iyoda, M. *Heteroatom Chem.* **2007**, *18*, 460−466. (c) Hasegawa, M.; Iyoda, M. *Chem. Soc. Rev.* **2010**, *39*, 2420−2427.

(19) (a) Leu, W. C. W.; Fritz, A. E.; Digianantonio, K. M.; Hartley, C. S. *J. Org. Chem.* **2012**, *77*, 2285−2298. (b) Jurow, M.; Schuckman, A. E.; Battteas, J. D.; Drain, C. M. *Coord. Chem. Rev.* **2010**, *254*, 2297−

2310. (c) Weibel, N.; Mishchenko, A.; Wandlowski, T.; Neuburger, M.; Leroux, Y.; Mayor, M. *Eur. J. Org. Chem.* **2009**, 6140−6150.
(20) (a) Iyoda, M. *Adv. Synth. Catal.* **2009**, *351*, 984−998. (b) Kawase, T. *Synlett* **2007**, 2609−2626. (c) MacLachlan, M. J. *Pure Appl. Chem.* **2006**, *78*, 873−888. (d) Kaiser, A.; Bäuerle, P. *Top. Curr. Chem.* **2005**, *249*, 67−125.
(21) (a) Hu, Z.; Atwood, J. L.; Cava, M. P. *J. Org. Chem.* **1994**, *59*, 8071−8075. (b) Kawase, T.; Darabi, H. R.; Uchimiya, P.; Oda, M. *Chem. Lett.* **1995**, 499−500.
(22) For vanadium-catalyzed pinacol coupling and Corey−Winter reaction: Kuwatani, Y.; Yoshida, T.; Hara, K.; Yoshida, M.; Matsuyama, H.; Iyoda, M. *Org. Lett.* **2000**, *2*, 4017−4020.
(23) Intramolecular cyclization of **5** may produce *E*- and *Z*-**7**, in which *Z*-**7** is 8.4 kcal/mol more stable than *E*-**7**, as determined from B3LYP/6-31G(d,p) calculations.
(24) The diastereomeric selectivity of the reaction was high, and only (*Z*,*Z*)-**1**, (*E*,*E*,*E*)-**2**, and (*E*,*E*,*E*,*E*)-**3** were obtained without the formation of other diastereomers.
(25) DFT calculations on **9** showed an exactly planar structure as an energy minimum despite the very close S(2)···S(3) distance (3.178 Å) (Figure S14a, Supporting Information).
(26) DFT calculations on **9** also showed a twisted conformation as a local minimum (Figure 14b, Supporting Information). Total energy of the twisted conformer of **9** is higher than that of the planar structure by 4.93 kcal mol^{-1}.
(27) For crystal structure of macrocycles: Grave, C.; Lentz, D.; Schäfer, A.; Samori, P.; Rabe, J. P.; Franke, P.; Schlüter, A. D. *J. Am. Chem. Soc.* **2003**, *125*, 6097−6918.
(28) X-ray analysis of the macrocyclic oligothiophene 4-mer also showed a nonplanar twisted structure: Iyoda, M.; Huang, P.; Nishiuchi, T.; Takase, M.; Nishinaga, T. *Heterocycles* **2011**, *82*, 1143−1149.
(29) Lazzaroni, R.; Calderone, A.; Lambin, G.; Rabe, J. P. *Synth. Met.* **1991**, *41*, 525−528.
(30) (a) Puigmartí-Luis, J.; Minoia, A.; Uji-i, H.; Rovira, C.; Cornil, J.; De Feyter, S.; Lazzaroni, R.; Amabilino, D. B. *J. Am. Chem. Soc.* **2006**, *128*, 12602−12603. (b) Glowatzki, H.; Gavrila, G. N.; Seifert, S.; Johnson, R. I.; Räder, J.; Müllen, K.; Zahn, D. R. T.; Rabe, J. P.; Koch, N. *J. Phys. Chem. C* **2008**, *112*, 1570−1574. (c) Sakano, T.; Hasegawa, J.; Higashiguchi, K.; Matsuda, K. *Chem. Asian J.* **2012**, *7*, 394−399.
(31) Samolí, P.; Severin, N.; Simpson, C. D.; Müllen, K.; Rabe, J. P. *J. Am. Chem. Soc.* **2002**, *124*, 9454−9457.
(32) Each oxidation step for **2**−**4** involved a one-electron process based on peak-to-peak potential separations (59−76 mV), whereas the narrower peak-to-peak potential separation (49 mV) of **1** compared with that of ferrocene, which showed 63 mV under the same conditions, strongly suggested a two-electron oxidation process. The two-electron oxidation process was also supported by rotating disc electrode voltammetry of **1** (see Figure S9, Supporting Information).
(33) (a) Bond, A. M.; McLennan, E. A.; Stojanovic, R. S.; Thomas, F. G. *Anal. Chem.* **1987**, *59*, 2853−2860. (b) Trasalti, S. *Pure Appl. Chem.* **1986**, *58*, 956−966. (c) Cardona, C. M.; Li, W.; Kaifer, A. E.; Stockdale, D.; Bazan, G. C. *Adv. Mater.* **2011**, *23*, 2367−2371.
(34) Although **1**, **2**, and **4** have potential paramagnetic 36π and 54π systems, almost no paratropicity was observed in their ^{1}H NMR spectra (Figures S1, S3, and S5, Supporting Information).
(35) (a) Nakano, M.; Kishi, R.; Nitta, T.; Kubo, T.; Nakasuji, K.; Kamada, K.; Ohta, K. *J. Phys. Chem. A* **2005**, *109*, 885−891. (b) Kamada, K.; Ohta, K.; Kubo, T.; Shimizu, A.; Morita, Y.; Nakasuji, K.; Kishi, R.; Ohta, S.; Furukawa, S.; Takahashi, H.; Nakano, M. *Angew. Chem., Int. Ed.* **2007**, *46*, 3544−3546. (c) Konishi, A.; Hirao, Y.; Nakano, M.; Shimizu, A.; Botek, E.; Champagne, B.; Shiomi, D.; Sato, K.; Takui, T.; Matsumoto, K.; Kurata, H.; Kubo, T. *J. Am. Chem. Soc.* **2010**, *132*, 11021−11023.
(36) For $Fe(ClO_4)_3$ oxidation: Hasegawa, M.; Enozawa, H.; Kawabata, Y.; Iyoda, M. *J. Am. Chem. Soc.* **2007**, *129*, 3072−3073.
(37) For UV−vis−NIR spectra of macrocyclic cationic species: (a) Zhang, F.; Götz, G.; Mena-Osteritz, E.; Weil, M.; Sarkar, B.; Kaim, W.; Bäuerle, P. *Chem. Sci.* **2011**, *2*, 781−784. (b) Golder, M. R.; Wong, B. M.; Jasti, R. *Chem. Sci.* **2013**, *4*, 4285−4291.
(38) Our experimental findings on the UV−vis−NIR spectra were supported by theoretical calculations (Figure S30−S32, Supporting Information).
(39) (a) Levillain, E.; Roncali, J. *J. Am. Chem. Soc.* **1999**, *121*, 8760−8765. (b) Raimundo, J.-M.; Levillain, E.; Gallego-Planas, N.; Roncali, J. *Electrochem. Commun.* **2000**, *2*, 211−215. (c) Tateno, M.; Takase, M.; Iyoda, M.; Komatsu, K.; Nishinaga, T. *Chem.—Eur. J.* **2013**, *19*, 5457−5467.
(40) The first decrease of the ESR signal is due to the solvent effect of CH_2Cl_2, and the increase at −113 °C is due to a usual Curie bahavior.
(41) Döhnert, D.; Koutecký, J. *J. Am. Chem. Soc.* **1980**, *102*, 1789−1796.
(42) Schleyer, P. v. R.; Maerker, C.; Dransfeld, A.; Jiao, H.; Hommes, N. J. R. v. E. *J. Am. Chem. Soc.* **1996**, *118*, 6317−6318.
(43) **1** exhibited no liquid crystalline property, as observed by polarization microscopy.
(44) The DSC behavior of **1** with different crystals under the same conditions was reproducible. However, using the same cooling process (2 °C/min), the exothermic peak became larger and shifted to higher temperature as the heating rate was increased (Figure S34a, Supporting Information). Using the same heating process (2 °C/min), the exothermic peak became smaller as the cooling rate was increased (Figure S34b, Supporting Information).
(45) Because the molecular diameter of **1** was estimated to be a maximum of 26 Å, the XRD profile shows a laterally ordered lamellar structure (d = 21.0 Å) that rises 54° diagonally from the aluminum plate.
(46) Cast films of **2**, **3**, and **4** from benzene or toluene have an amorphous morphology; however, recrystallization of **2**, **3**, and **4** from CH_2Cl_2−ethyl acetate affords fine crystals. These crystals also exhibit no polymorphism presumably owing to the planar π−π stacking structure.
(47) The known macrocyclic oligothiophene 4-mers also show two different crystalline state structures owing to either favorable molecular packing or stabilization with π−π stacking. Although the oligothiophene 4-mer with butyl substituents showed a twisted crystal structure in response to favorable molecular packing,[28] X-ray analysis of a similar oligothiophene 4-mer without a substituent revealed a stacked planar structure stabilized by π−π stacking interaction despite very short S···S distances (3.014(2) and 3.025 Å): Kawase, T.; Darabi, H. R.; Uchimiya, R.; Oda, M. *Chem. Lett.* **1995**, 499−500.
(48) The single crystals of **1** showed stronger emission in the solid state (λ_{em} = 603 nm, Φ_F = 0.026) with a broad absorption at λ_{max} = 380 nm, owing to the rigid twisted structure with a weak intermolecular interaction.
(49) UV−vis and fluorescence spectra of **LC-1** show a redshift of absorption and emission maxima (Figures S35−S37, Supporting Information).